

# Numerical Simulation of H<sub>2</sub> Addition Effect to CH<sub>4</sub> Premixed Turbulent Flames for Gas Turbine Burner

S. Ouali<sup>†</sup>

LEMI laboratory, Faculty of technology, M'hammed Bougara University, Frantz Fanon street, 35 100 Boumerdes, Algeria

<sup>†</sup>Corresponding Author Email: [s.ouali@univ-boumerdes.dz](mailto:s.ouali@univ-boumerdes.dz)

## ABSTRACT

Present computational simulation studied H<sub>2</sub>-CH<sub>4</sub> combustion characteristics in a specific gas turbine combustor used for power generation. Across four thermal loads (1.1-4.4 bar) and varying hydrogen fraction (0-50% by volume), changes in flame temperature, reaction zone stability, and flow field are scrutinized. Results show coherent thermal patterns and stable flame fronts across all conditions, indicating hydrogen addition does not deteriorate combustion when blended with methane. Flame temperatures increase by approximately 40 K with increasing hydrogen fraction. Acceptable NO<sub>x</sub> emissions are observed, peaking at 6.20 ppm with 50 % H<sub>2</sub> at 168 kW. The combustor enables reliable operation for blends up to 50% hydrogen. These results suggest potential for increasing legislated hydrogen blending limits for more sustainable gas turbine power generation. By expanding the viable envelope for hydrogen-methane mixtures, this work contributes to understanding combustion of decarbonized fuels in gas turbines. However, as results are limited to the investigated combustor geometry, generalized conclusions cannot be drawn at this stage. Nonetheless, this study represents an incremental advancement in knowledge that may inform future research on sustainable power generation and decarbonization efforts.

## Article History

Received November 23, 2023

Revised February 25, 2024

Accepted March 8, 2024

Available online May 29, 2024

## Keywords:

Hydrogen-Methane  
High pressure burners  
Swirled flames  
Gas turbine  
Pollutants

## 1. INTRODUCTION

In response to escalating global energy demands and the imperative to address global warming, the scientific community is compelled to explore alternative energy sources. This exploration seeks to meet surging energy needs while maintaining environmental sustainability. Among the promising avenues is the utilization of hydrogen, particularly as a blended fuel with conventional fuels. This blending not only holds the potential for a substantial reduction in pollutant emissions, contributing to the decarbonization initiative, but also offers cost-effective benefits. The integration of hydrogen into existing facilities, particularly in electricity generation using methane-powered gas turbines, presents an opportunity for both environmental sustainability and economic feasibility. Additionally, hydrogen serves as a means of energy storage sourced from renewable origins.

Our current work aligns with this critical domain, involving a numerical simulation of hydrogen-methane flames within a second-generation high-pressure generic swirl burner (HPGSB). A careful study of flame behavior in this burner geometry can provide insights leading to impactful advancements in sustainable power generation.

The focus lies on the effects of hydrogen addition up to 50% by volume and the elevation of reactant inlet pressure, translating to an increase in power from 42 kW to 168 kW. The scrutiny encompasses flow field characteristics, temperature distribution, flame locations, and NO<sub>x</sub> emissions. The HPGSB burner, as depicted in Fig. 1, was developed by researchers at Cardiff University and subjected to extensive experimentation (Syred et al., 2015). These experiments covered varying power ranges typical of burners used in gas turbines, diverse fuel blends,

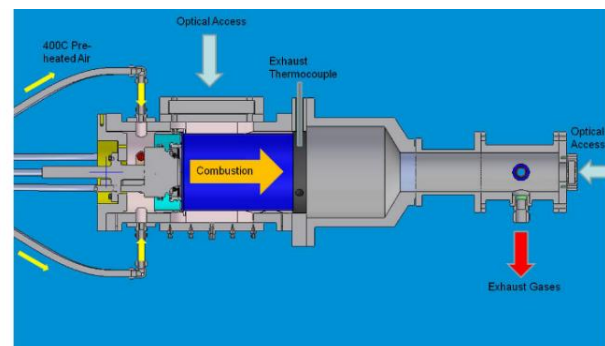


Fig.1 Combustor configuration

NOMENCLATURE			
$A'$	combustion model constant	$u'$	RMS velocity
$c$	mean progress variable	$Y_M$	compressible turbulence dissipation term
$C_2, C_{1e}$	turbulence model constants	$z$	axial coordinate
$F_i$	external forces in i-direction	$\alpha$	volumetric concentration of H <sub>2</sub>
$g_i$	gravitational acceleration in i-direction	$\varepsilon$	turbulent kinetic energy dissipation
$G_k, G_b$	turbulence kinetic energy generation terms	$\phi$	fuel-air equivalence ratio
$k$	turbulent kinetic energy	$U_l$	laminar flame speed
$l_t$	turbulence length scale	$u'$	RMS velocity
$p$	mean pressure	$Y_M$	compressible turbulence dissipation term
$r$	radial coordinate	$\rho$	fluid density
$S_k, S_\varepsilon$	source terms	$\vec{v}$	velocity vector
$S_c$	progress source term	$\sigma_k, \sigma_\varepsilon$	turbulent Prandtl numbers
$Sc_t$	turbulent Schmidt number	$\mu$	viscosity
$u'$	RMS velocity	$\mu_t$	turbulent viscosity
$U_l$	laminar flame speed		

and compositions, as well as iterative modifications to the burner's geometry. The results showcased the burner's operational flexibility while maintaining stable functionality within pollution thresholds defined by regulations.

While gas turbines remain indispensable for electricity generation, their pollutant emissions pose significant environmental and health risks. As a response, scientists are dedicated to the development of combustion technologies with low pollutant emission rates. The ensuing literature review synthesizes major research findings on combustion in burners used in gas turbines, providing valuable perspectives on advances in this important domain.

Geometric and design analysis is crucial as several research results assert that burner geometry substantially impacts flame structures and consequently pollutant emissions. Key parameters in geometry design include swirl number, nozzle design, the number of swirl vanes, and combustion chamber proportions relative to the exit nozzle (Baej et al., 2018; Runyon et al., 2020; Adamou et al., 2021; Mahto & Chakravarthy, 2022; Moraes et al., 2022). For instance, an optimal swirl number can enhance flame stability, owing to amplified turbulence inducing faster flame speeds (İlbaş et al., 2016; Ouali et al., 2016; Rajabi & Amani, 2019). Additionally, the shape of the burner exit nozzles (converging and diverging) considerably affects the size of generated vortices, affecting the shear layer and hence the velocity field. Even the size of the swirl-generating nozzles has an effect on the resulting combustion products and velocity distribution via temperature changes (Murthy et al., 2018; Lokini et al., 2019). The reaction zone length is largely affected; however, increasing the combustion chamber length results in a substantial variation of flame structures, related to the flow attachment surface area on the walls. The porosity of the studied burner nozzle surfaces has shown major importance in flame structures as well as NO<sub>x</sub> emissions – higher porosity promotes reduced NO<sub>x</sub> associated with lower flame temperatures and residence times (Runyon, 2017; Masroui et al, 2023; Psomoglou, 2023). These findings emphasize that rigorous numerical and experimental investigations are necessary to propose an optimal and effective burner geometry in terms of flame

stability, system durability, and lowered pollutant emissions.

In terms of imaging technics, current technological advancements enable the use of highly advanced and accurate imaging technologies in combustion analysis. Experimental studies on gas turbine combustors extensively leverage these techniques. Chemiluminescence is utilized specifically to locate chemical radicals that enable precise identification of flame front positions, with very high accuracy levels. Localizing CH\* and OH\* radicals defines the flame stability level, thereby enabling stability optimization (Boxx et al., 2015; Lee et al., 2015; Valera-Medina et al., 2017; Zhang et al., 2018). Additionally, high-speed imaging sampling increases the accuracy of studied parameters, such as examining the impact of pressure on combustion quality conducted by Kruse et al. (2015) and Emami et al. (2019). Laser application has enabled investigating several parameters influencing flame behavior. Its use in this field has improved our comprehension of how various factors like O<sub>2</sub> concentration, turbulence level, and reactive mixture composition impact pollutants, flame front structures and positions, velocity fields, heat release rates, and turbulence levels (Chen & Driscoll, 2016; Liu et al., 2017; Valera-Medina et al., 2017; Nemitallah et al., 2018). These approaches can be listed as OH\* and CH\* chemiluminescence, particle image velocimetry (PIV), planar laser-induced fluorescence (PLIF), laser spectroscopy, shadowgraphy, and laser Doppler anemometry (LDA).

Numerous HPGSB studies have investigated the compositions of injected fuels to evaluate burner operational flexibility and improve performance while reducing polluting emissions. Several mixtures have been tested: H<sub>2</sub>O vapor, biogas, H<sub>2</sub>, H<sub>2</sub>-CH<sub>4</sub>, H<sub>2</sub>-CH<sub>4</sub>-NH<sub>3</sub>, and syngas. Results indicate that low concentrations of NH<sub>3</sub>-H<sub>2</sub> or NH<sub>3</sub>-CH<sub>4</sub> promote NO<sub>x</sub> compared to pure CH<sub>4</sub>. However, as the NH<sub>3</sub> content increases, CO and unburnt hydrocarbons (UHC) appearance also rises due to decreased combustion temperatures (Valera-Medina et al., 2017; Kurata et al., 2019; Li et al., 2019; Okafor et al., 2019). Additionally, adding H<sub>2</sub>O vapor showed increased flame speeds, enhancing combustion stability while

minimizing pollutant formation (Amani et al., 2018; Runyon et al., 2020; Reale & Sannino, 2021). Pashchenko (2024) tested 100% NH<sub>3</sub>, but the results were not encouraging. Biogas and biodiesel were also examined by Liu et al. (2020), Benaissa et al. (2022), and Agwu et al. (2020); they found NO<sub>x</sub> augmentation with a slight decrease in O<sub>2</sub> and CO in the exhaust.

The development of current computational tools has enabled several studies to utilize numerical simulations to obtain valuable insights into combustion phenomena, particularly in HPGSBs. Using large eddy simulation (LES), the prediction of chemical species like CO and NO<sub>x</sub> emissions, unburnt hydrocarbons (UHC), CO, and soot is highly accurate. Furthermore, dynamic and thermal fields are predicted with very acceptable precision. Turbulence models coupled with combustion models provide quality predictions of turbulent flames (Bulat et al., 2015; Runyon et al., 2020). The numerical approach combined with experimental work offers an important alternative for advancing knowledge of HPGSB combustion. Advanced simulations provide detailed characterization of flame properties, emissions, and fluid behaviors. Validation against lab data and iteration with experiments enables optimized burner designs. Ongoing refinement of chemical kinetic mechanisms in models will further improve reliability. Numerical techniques present a powerful tool, complementing physical testing, to unravel combustion intricacies in high-pressure systems (See & Ihme, 2015).

Physical parameter effects have been extensively investigated in studies on gas turbine combustors. Inlet temperature and pressures are examined extensively given these burners must operate at variable loads typical of gas turbine systems. Results from Runyon et al. (2020) indicate that increasing inlet pressure and operating power enhance combustion quality by raising reaction rates and decreasing residence time. However, this improvement is conditioned by increased NO<sub>x</sub> emissions. Conversely, Chen et al. (2019) proved that elevating inlet temperature promotes flashback occurrences and flame instabilities.

Finally, works on gas turbine combustors have comprehensively examined geometric and parametric effects using experimental and numerical approaches, enabling enhanced understanding of gas turbine combustion. Our study aims to further enrich knowledge in this domain. Results on hydrogen addition to methane up to 50% will quantify H<sub>2</sub> limits to avoid. These concentrations will be tested at four inlet pressures (1.1 to 4.4 bar) to reproduce realistic burner operating condition. The concentration range is chosen based on current regulations (Erdener et al., 2023). By scrutinizing flame behavior, flow fields, temperatures, and emissions with incremental hydrogen fraction under practical conditions, our simulations will uncover viability thresholds for clean power generation. The data will inform blend optimization strategies to balance performance and pollutants. While cognizant of the model limitations, these insights can guide the development of sustainable gas turbine technologies. Our contributions complement the established knowledge base, providing an incremental

step toward decarbonized combustion systems in the pursuit of environmentally sustainable power generation.

## 2. NUMERICAL APPROACH

### 2.1 Numerical Setup

The turbulent premixed H<sub>2</sub>-CH<sub>4</sub> flames were numerically simulated using ANSYS Fluent software, which solves the Navier-Stokes equations by discretizing the computational domain with the finite volume method. The pressure-based solver was used for its robustness in modeling incompressible flows. Velocity-pressure coupling was ensured by the SIMPLE algorithm to enable stable convergence. Second-order spatial discretization with the Upwind scheme improved solution accuracy. A steady-state approach was warranted since the investigated flames exhibit no temporal evolution. Convergence was attained when residuals dropped below 10<sup>-6</sup>, except for continuity (10<sup>-4</sup>).

### 2.2 Governing Equations and Models

Reactive flows are governed by equations of fluid mechanics coupled with those of combustion. Employing Ansys Fluent software with the RANS (Raynolds Averaged Navier-Stokes) approach, solving this system of equations was required (Eq. (1) and Eq. (2)):

The conservation of mass:

$$\frac{\partial \rho}{\partial t} + \nabla \cdot (\rho \vec{v}) = 0 \quad (1)$$

The momentum equation is:

$$\frac{\partial}{\partial t} (\rho \tilde{u}_i) + \frac{\partial}{\partial x_j} (\rho \tilde{u}_i \tilde{u}_j) = -\frac{\partial}{\partial x_i} (p + \rho k) + \frac{\partial}{\partial x_j} \left( \mu \frac{\partial \tilde{u}_i}{\partial x_j} \right) + \rho g_i + F_i \quad (2)$$

Turbulence was modeled with the RANS Realizable k-epsilon, recommended for swirling flows (ANSYS Fluent Theory Guide, Release 17.2, ANSYS, Inc). In this model, two transport equations are solved for k and epsilon (Eqs. (3) and (4)). The modified turbulent viscosity formulation is given in equation 5.

$$\frac{\partial}{\partial t} (\rho k) + \frac{\partial}{\partial x_j} (\rho k u_j) = \frac{\partial}{\partial x_j} \left[ \left( \mu + \frac{\mu_t}{\sigma_k} \right) + \frac{\partial k}{\partial x_j} \right] + G_k + G_b - \rho \epsilon - Y_M + S_k \quad (3)$$

$$\frac{\partial}{\partial t} (\rho \epsilon) + \frac{\partial}{\partial x_j} (\rho \epsilon u_j) = \frac{\partial}{\partial x_j} \left[ \left( \mu + \frac{\mu_t}{\sigma_\epsilon} \right) + \frac{\partial \epsilon}{\partial x_j} \right] + \rho C_1 S_\epsilon - \rho C_2 \frac{\epsilon^2}{k + \sqrt{\nu \epsilon}} + C_{1\epsilon} \frac{\epsilon}{k} C_{3\epsilon} G_b + S_\epsilon \quad (4)$$

$$\mu_t = \rho C_\mu \frac{k^2}{\epsilon} \quad (5)$$

The Partially Premixed combustion model was utilized for this analysis. The present implementation combines the Zimont method for evaluating turbulent flame speed (TFS) (equation (6)), Progress Variable equation for 'c' (equation (7)), and equilibrium PDF (probability density function) approach for chemical species analysis (equation (8)).

The calculation equation for TFS:

$$U_t = A (\dot{u})^{3/4} U_l^{1/2} \alpha^{-1/4} l_t^{1/4} \quad (6)$$

The progress variable transport equation is:

$$\frac{\partial}{\partial t}(\rho \bar{c}) + \nabla \cdot (\rho \vec{v} \bar{c}) = \nabla \cdot \left( \left( \frac{k}{c_p} + \frac{\mu_t}{Sc_t} \right) \nabla \bar{c} \right) + \rho S_c \quad (7)$$

The progression variable 'c' defines the reaction progress rate and flame front positioning. A value of 0 indicates the unburned mixture zone while 1 denotes the burned zone. The flame front is typically located at 'c' values between 0.4 and 0.6 (the reaction zone).

The density weighted mean scalars  $\phi$  are calculated from:

$$\bar{\phi} = \int_0^1 \int_0^1 \phi(f, c) f(f, c) dc df \quad (8)$$

Where f and c are the PDF variables,  $\phi(f, c)$  is the scalar value at a specific point in the f-c space and f(c, f) is the PDF at the same point.

In this modeling approach, the temperature T is computed through:

$$p = \rho(C) R T \quad (9)$$

T(C) is obtained from Gibbs equilibrium, and the average T(C) provides the temperature field.

NOx emissions were predicted with the NOx model (equation 10), accounting for prompt, fuel and thermal NOx formation (Eqs. (11-13)).

The NOx conservation equation is:

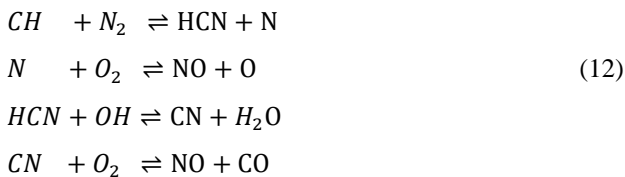
$$\frac{\partial}{\partial t}(\rho Y_\theta) + \nabla \cdot (\rho \vec{v} Y_\theta) = \nabla \cdot (\rho D \nabla Y_\theta) + S_\theta \quad (10)$$

where  $Y_\theta$  denotes NO, HCN, NH<sub>3</sub> and N<sub>2</sub>O mass fractions.

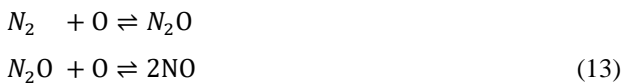
Thermal NOx mechanisms is:



Prompt NOx mechanisms is:



Intermediate NOx mechanism is:



All the equations mentioned in this section have been taken from ANSYS Fluent theory guide ([ANSYS Fluent Theory Guide, Release 17.2, ANSYS, Inc. 2016](#)).

### 2.3 Computational Domain

This numerical simulation utilizes the second generation HPGSB designed by Cardiff University ([Runyon, 2017](#)). The dimensions and details of the 3D computational domain are depicted in Fig. 2.

The combustor features a cylindrical geometry (434 mm length and 100 mm radius) and a uniform (non-

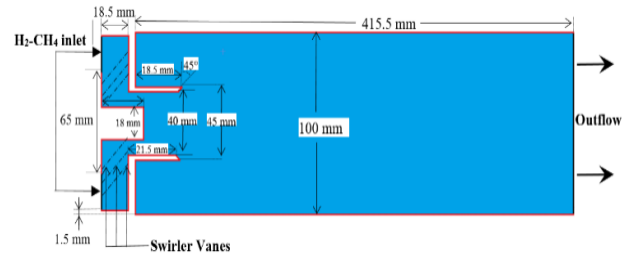


**Fig. 2 Axial geometric cross section of the computational domain**

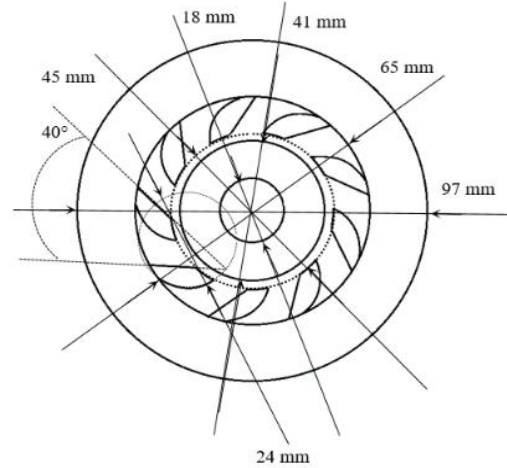


**Fig. 3 Burner nozzle (swirler)**

converging) exit shape. The premixed reactants flow through the inlet nozzle (swirler) containing 9 vanes that generate swirl (Fig. 3). This domain comprises a single annular inlet and an axial outlet.

### 2.4 Mesh Study

Figure 4 illustrates the grid nature adopted. Refinement occurred near the inlet nozzle and lateral walls where variations in physical variables are substantial (reaction zone). This refinement also enables proper turbulence model functionality. The generated elements are hexagonal with minimal size variation (due to grid refinement). This quality mesh enables improved stability and accuracy.

The selected grid was based on a grid independence study. Various refinements were tested, starting with 300000 elements up to 2 million. The impact on velocity and temperature distribution dictated the choice.

Temperature profiles at the burner outlet in Fig. 5 demonstrate result sensitivity to element numbers. Above 1 million elements, variations became minimal. No important difference existed between 1.75 and 2 million elements. To ensure high accuracy, the 1.75 million element grid was selected.

The same finding applied when analyzing Fig. 6. Velocity was inspected on two radial sections: (a) the centerline and (b) 50 mm radially from the nozzle outlet. These curves confirmed the 1.75 million element grid for the study.

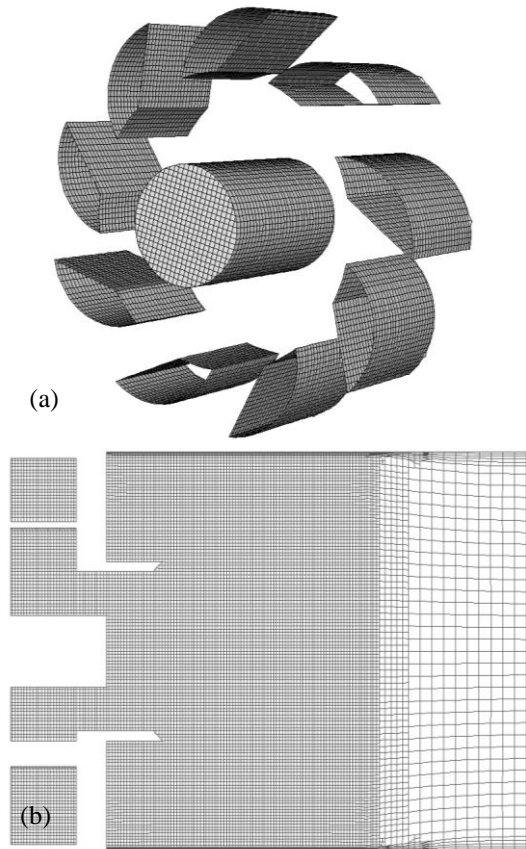


Fig. 4 Mesh Visualization: (a) Swirler valves, (b) Axial cross-section view of the Domain

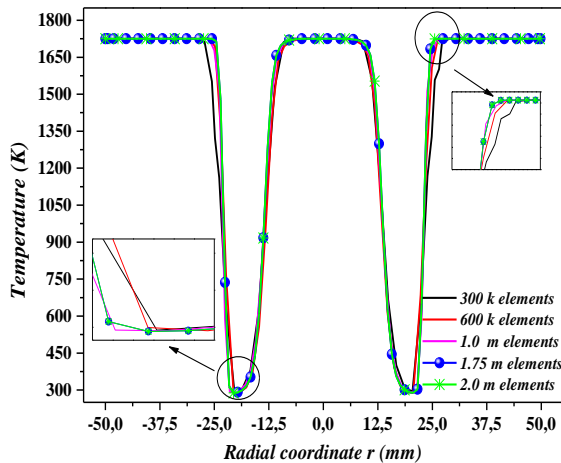


Fig. 5 Temperature variations at nozzle outlet across multiple mesh arrangements

### 2.5 Adjustment of Numerical Parameters

This work elucidates hydrogen addition impact to methane in HPGSB combustor across four power levels. Numerous calculations defined the fuel mixture properties.

Concentrations of H<sub>2</sub> were varied within the range of 0% to 50% (volume percentage of H<sub>2</sub>: Vol % H<sub>2</sub>). This was done four absolute inlet pressures: 1.10 bar, 2.20 bar, 3.30 bar, and 4.40 bar. These directly represent power levels ranging from 42 kW to 168 kW.

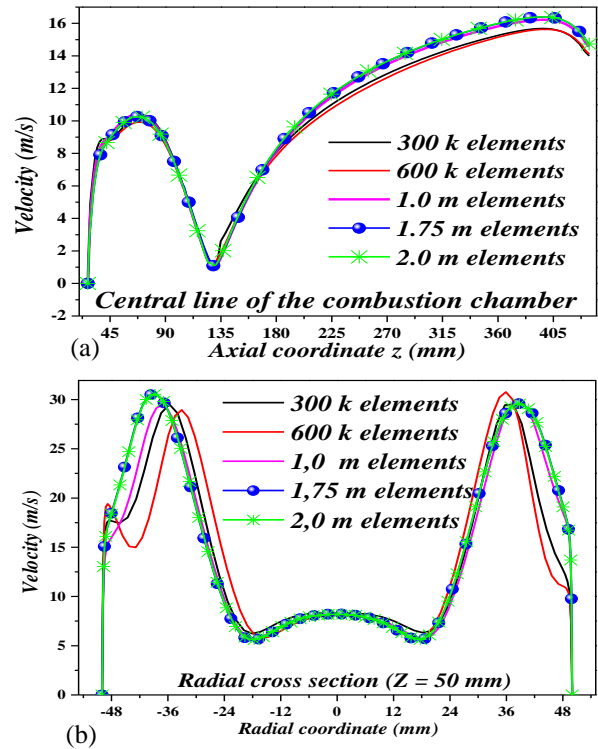


Fig. 6 Velocity variation at different positions for multiple tested grids

Mass fractions accounting for H<sub>2</sub> variation were computed using equations (14) and (15).

$$(1 - \alpha)CH_4 + \alpha H_2 + \left(x - \frac{3}{2}\alpha + 2\right) (O_2 + 3.76 N_2) \quad (14)$$

$$x = (3/2)\alpha + ((2 - (3/2)\alpha)/\phi) - 2 \quad (15)$$

Thermal conductivity ( $\lambda$ ) and dynamic viscosity ( $\eta$ ) were calculated using Gazeq software to ensure combustion model (PDF) accuracy. Heating values (LCV) were re-evaluated for each blend to maintain the stated power levels. This required re-adjusting reactant flow rates per case, summarized in Tables 1 to 5 for the four absolute pressures.

Table 1 Properties of the fuel mixture

Vol % H <sub>2</sub>	$\lambda$ , W.m <sup>-1</sup> .K <sup>-1</sup>	$\eta$ , Pa.s (1 <sup>e</sup> -5)	LCV, MJ.kg <sup>-1</sup>
0	0.0415	2.86	50.03
5	0.0463	2.86	50.49
10	0.0512	2.86	51.26
15	0.0561	2.85	51.55
20	0.0612	2.85	52.16
25	0.0662	2.84	52.84
30	0.0711	2.84	53.61
35	0.0766	2.83	54.47
40	0.0819	2.82	55.44
45	0.0873	2.81	56.56
50	0.0931	2.89	57.85

**Table 2 Parameters for the 42 kW case - inlet pressure set at 1.1 bar**

Vol % H <sub>2</sub>	MFR, g.s <sup>-1</sup>	MF CH <sub>4</sub>	MF H <sub>2</sub>	MF O <sub>2</sub>	MF N <sub>2</sub>
0	27.13	3.093	0	22.497	74.409
5	27.06	3.054	0.020	22.502	74.424
10	26.97	3.011	0.041	22.507	74.441
15	26.88	2.965	0.065	22.512	74.458
20	26.79	2.914	0.091	22.518	74.477
25	26.68	2.859	0.119	22.524	74.498
30	26.57	2.798	0.150	22.531	74.521
35	26.44	2.731	0.184	22.539	74.546
40	26.31	2.657	0.221	22.547	74.574
45	26.16	2.575	0.263	22.556	74.605
50	25.99	2.482	0.310	22.567	74.640

**Table 3 Parameters for the 84 kW case - inlet pressure set at 2.2 bar**

Vol % H <sub>2</sub>	MFR, g.s <sup>-1</sup>	MF CH <sub>4</sub>	MF H <sub>2</sub>	MF O <sub>2</sub>	MF N <sub>2</sub>
0	54.27	3.093	0	22.497	74.409
5	54.12	3.054	0.0200	22.502	74.424
10	53.95	3.011	0.0418	22.507	74.441
15	53.77	2.965	0.0653	22.512	74.458
20	53.58	2.914	0.0910	22.518	74.477
25	53.37	2.859	0.119	22.524	74.498
30	53.14	2.798	0.150	22.531	74.521
35	52.89	2.731	0.184	22.539	74.546
40	52.62	2.657	0.221	22.547	74.574
45	52.32	2.575	0.263	22.556	74.605
50	51.98	2.482	0.310	22.567	74.640

**Table 4 Parameters for the 126 kW case - inlet pressure set at 3.3 bar**

Vol % H <sub>2</sub>	MFR, g.s <sup>-1</sup>	MF CH <sub>4</sub>	MF H <sub>2</sub>	MF O <sub>2</sub>	MF N <sub>2</sub>
0	81.41	3.093	0	22.497	74.409
5	81.18	3.054	0.020	22.502	74.424
10	80.93	3.011	0.041	22.507	74.441
15	80.66	2.965	0.065	22.512	74.458
20	80.37	2.914	0.091	22.518	74.477
25	80.06	2.859	0.119	22.524	74.498
30	79.72	2.798	0.150	22.531	74.521
35	79.34	2.731	0.184	22.539	74.546
40	78.93	2.657	0.221	22.547	74.574
45	78.48	2.575	0.263	22.556	74.605
50	77.98	2.482	0.310	22.567	74.640

All tests were performed at a 573 K inlet temperature and equivalence ratio  $\phi = 0.55$ , eliminating their potential effects.

The boundary conditions employed:

- Inlet: mass flow
- Outlet: outflow
- All walls: adiabatic

**Table 5 Parameters for the 168 kW case - inlet pressure set at 4.4 bar**

Vol % H <sub>2</sub>	MFR, g.s <sup>-1</sup>	MF CH <sub>4</sub>	MF H <sub>2</sub>	MF O <sub>2</sub>	MF N <sub>2</sub>
0	108.55	30.93	0	22.497	74.409
5	108.24	30.54	0.020	22.502	74.424
10	107.91	30.11	0.041	22.507	74.441
15	107.55	29.65	0.065	22.512	74.458
20	107.17	29.14	0.091	22.518	74.477
25	106.75	28.59	0.119	22.524	74.498
30	106.29	27.98	0.150	22.531	74.521
35	105.79	27.31	0.184	22.539	74.546
40	105.24	26.57	0.221	22.547	74.574
45	104.64	25.75	0.263	22.556	74.605
50	103.97	24.82	0.310	22.567	74.64

The presented parameters enable a rigorous examination of flame behavior, temperatures, flow fields, and NO<sub>x</sub> emissions across a realistic operating envelope.

### 3. RESULTS AND DISCUSSIONS

#### 3.1 Validation of Mathematical Models

The numerical study of reactive flows requires the use of several mathematical models. Each has its own limitations and recommendations, in relation to the type of phenomenon studied and the nature of the results of interest (dynamic field, thermal fields or analysis of chemical species). Therefore, the more complex the phenomenon, the greater the number of models required for its analysis. This implies meticulous verification of the accuracy of combined models. For our work, the models used were validated with several experimental works available in the literature to cover a wide range of functionalities.

To ensure good prediction of the dynamic field, our numerical simulation was compared to experimental work available in the literature (Runyon, 2017).

Figure 7 illustrates the velocity of the present CFD study compared to those of the experimentation. Profiles were taken on a radial section for three different pressures; 1 bar, 2 bar and 3 bar. This pressure variation reflects the power variation, which further confirms the operational flexibility of HPGSBs in terms of power.

The Realizable variant of the k-epsilon model clearly reproduces the velocity distributions for all tested pressures with the experimental results. The profiles show very acceptable similarity. The maximum of the two variants (CFD and experimentation) coincides clearly (20 mm < z < 30 mm). Also, the negative values are located in the same places; in the center (-20 mm < z < 20 mm) and near the walls (42 mm < z < 50 mm). The central zone indicates the presence of a large central recirculation zone (CRZ) while that near the walls indicates the presence of two external recirculation zones (ORZ).

The second comparison we performed was to validate the combustion model used (PDF). Our results were

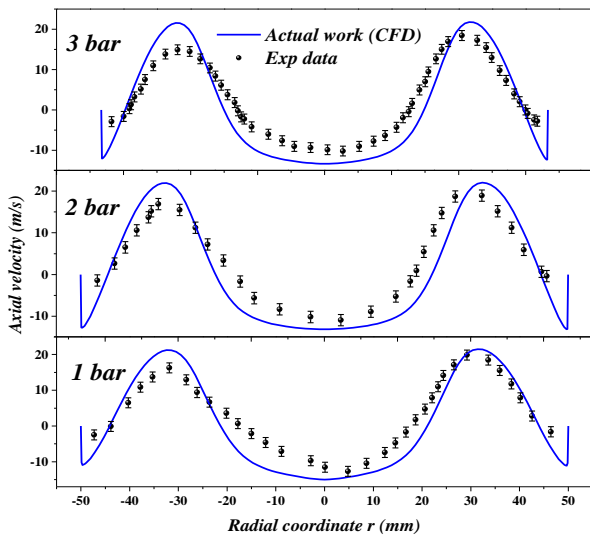


**Fig. 7** Comparison of axial velocities between CFD (actual work) and experimental measurements of Runyon (2017) for three selected pressures

compared with the experimental data from Runyon et al. (2020). Two reactant richnesses were tested (0.75 and 0.80) at constant power (25 kW).

The comparison parameter for the simulation is the progress variable 'c'. As defined in the second chapter (mathematical formulation of the combustion model), the progress variable 'c' indicates the reaction progression rate, the flame structure as well as the flame front position. While for the experimentation, the OH-radial was considered. Although mathematically these two variables ('c' and OH-radical) are not even similar, indication-wise we can use them to define the same parameters; flame structure and flame front positioning. Figure 8 shows the comparison made. These images indicate an acceptable similarity between the two approaches (CFD and experimentation). The length, inclination (angle  $\alpha$ ) and location of the flames appear very similar.

The results in Figure 8 encouraged us to use the PDF combustion model for the rest of this study.

One of the major aspects of our work is the prediction of NOx emissions which is a crucial aspect in the study of G.T combustors. For this, a comparison of the NOx rates predicted by CFD simulation was carried out with the results of Runyon (2017) (experimental data).

The NOx model used in ANSYS Fluent 17.2 is based on the exploitation of parameters (temperature, velocity and pressure) calculated by the turbulence-combustion model coupling to predict the NOx formation rate. This indicates that good NOx prediction reflects a good choice of the entire model combination used.

Two equations were necessary for the normalization of the NOx values obtained (equation 16 and equation 17). This normalization allows us to analyze the NOx rates relative to gas turbines in accordance with the ISO 11042 - 1: 1996 standards.

$$NO_{x,dry} = NO_{x,mean} / (1 - X_{H_2O}) \quad (16)$$

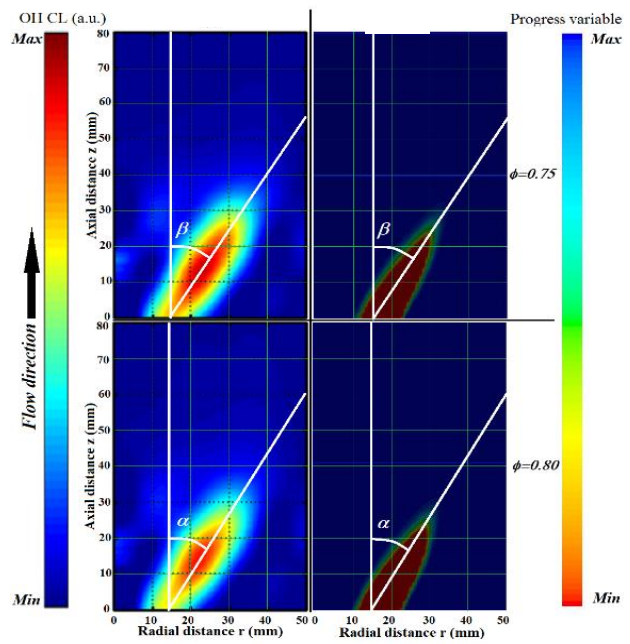


**Fig. 8** Flame front location – A comparative analysis between current CFD simulation (a) and experimental results by Runyon et al. (2020) for two different reactive mixture richness levels.

$$NO_{x,dry, 15\% O_2} = NO_{x,dry} * \left( \frac{20.9 - O_{2,ref}}{20.9 - O_{2,mean}} \right) \quad (17)$$

Where:

- NOx , mean: molar fraction (ppm)
- X<sub>H2O</sub>: mass fraction
- O<sub>2, ref</sub>: reel fraction of O<sub>2</sub> in the air
- O<sub>2, mean</sub>: computed fraction of O<sub>2</sub>.

The rates of NOx, H<sub>2</sub>O, and O<sub>2</sub> were considered at the outlet. This is to include all particles appearing in the combustion chamber. The parameters of the tests carried out are summarized in Table 6.

Figure 9 illustrates the comparison of the NOx predicted by this present numerical study with the experimental data from Runyon (2017). It is observed that for both tested fuels, the CFD results closely match those from the experimentation. For the first two pressures (1.1

**Table 6** Parameters for NOx model validation

Fuel composition	Inlet pressure, bar	Power, kW	Inlet T (k)	Swirl number S	$\phi$
- 0% H <sub>2</sub> - 100% CH <sub>4</sub>	1.1	42	573	0.8	0.55
	2.2	84			
	3.3	126			
- 15 % H <sub>2</sub> - 85 % CH <sub>4</sub>	1.1	42	573	0.8	0.55
	2.2	84			

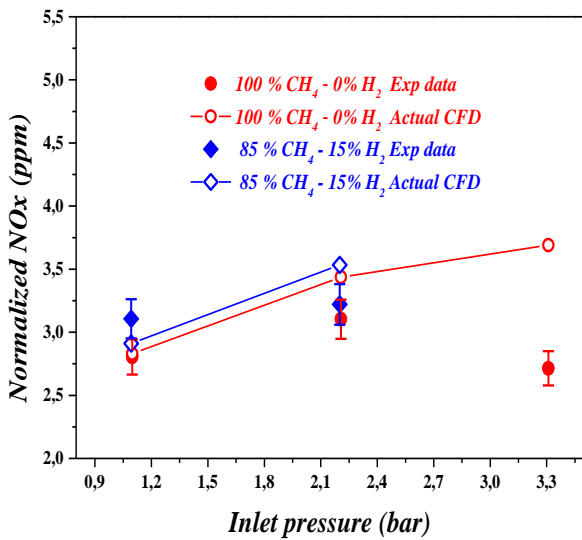


**Fig. 9** Normalized NOx emission rates for three input pressures (1.1, 2.2 and 3.3 bar) - A comparison of current CFD work and experimental data of Runyon (2017)

bar and 2.2 bar), the observed difference is negligible (<0.5 ppm). However, at 3.3 bar, a difference of approximately 1.07 ppm is noticed. This minor discrepancy is attributed to the "Adiabatic Walls" boundary condition assumed. As power increases, the temperature gradient rises. Therefore, the 'Adiabatic Walls' condition used tends to overpredict the temperature value and subsequent NOx formation. This assumption aimed to best reproduce the experimental test conditions, but will be revisited in future work.

Analysis of Fig. 9 supports continuing our study using the current combination of models.

Finally, this portion of the study provides encouragement to apply the stated mathematical models for analyzing H<sub>2</sub>-CH<sub>4</sub> combustion in HPGSB burners designed for gas turbines.

### 3.2 H<sub>2</sub> Impact on Temperature

To study the impact of adding H<sub>2</sub> to CH<sub>4</sub>, 44 numerical simulation cases were required. 11 cases for each inlet pressure (power level). The 11 cases represent the variation of the H<sub>2</sub> volumetric concentration (0% to 50%). Since the results are very similar (minimal variations), only three concentration cases will be shown in the figures (initial case: Vol% H<sub>2</sub> = 0%, intermediate case; Vol% H<sub>2</sub> = 50% and upper case: Vol% H<sub>2</sub> = 50%). This does not exclude discussing the remaining cases in the text. However, for the NOx analysis (section 3.4), the 44 simulation cases will be reported on the corresponding figure.

For the thermal field analysis, the temperature was evaluated on the longitudinal axis of the combustor (Fig. 10) and on three radial sections (Fig. 11) in addition to an overall view of the Progress Variable 'c' taken on a longitudinal surface cut of the computational domain (Fig. 12).

The curves plotted on Figure 10 indicate a proportional increase in adiabatic temperature flame

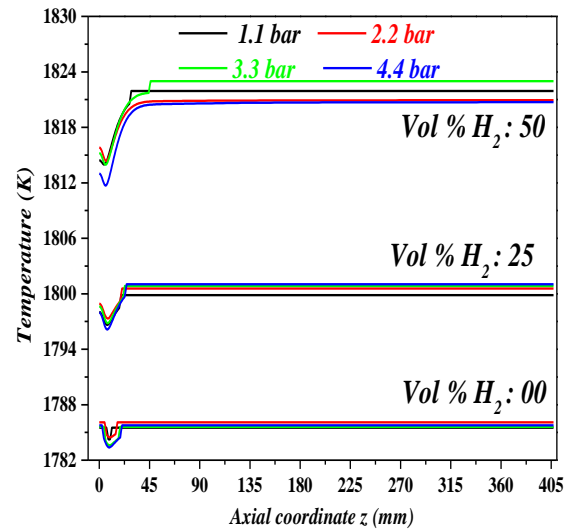


**Fig. 10** Impact of H<sub>2</sub> concentration on longitudinal temperature variations in the combustor (1.1, 2.2 and 3.3 bar)

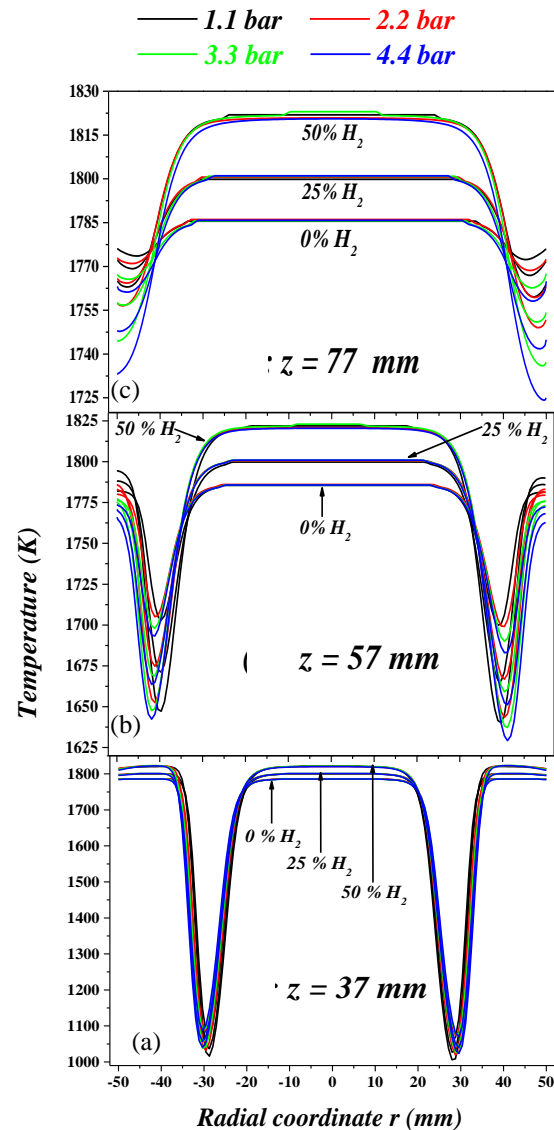


**Fig. 11** Impact of H<sub>2</sub> concentration on radial temperature profiles in the combustor (1.1, 2.2 and 3.3 bar)

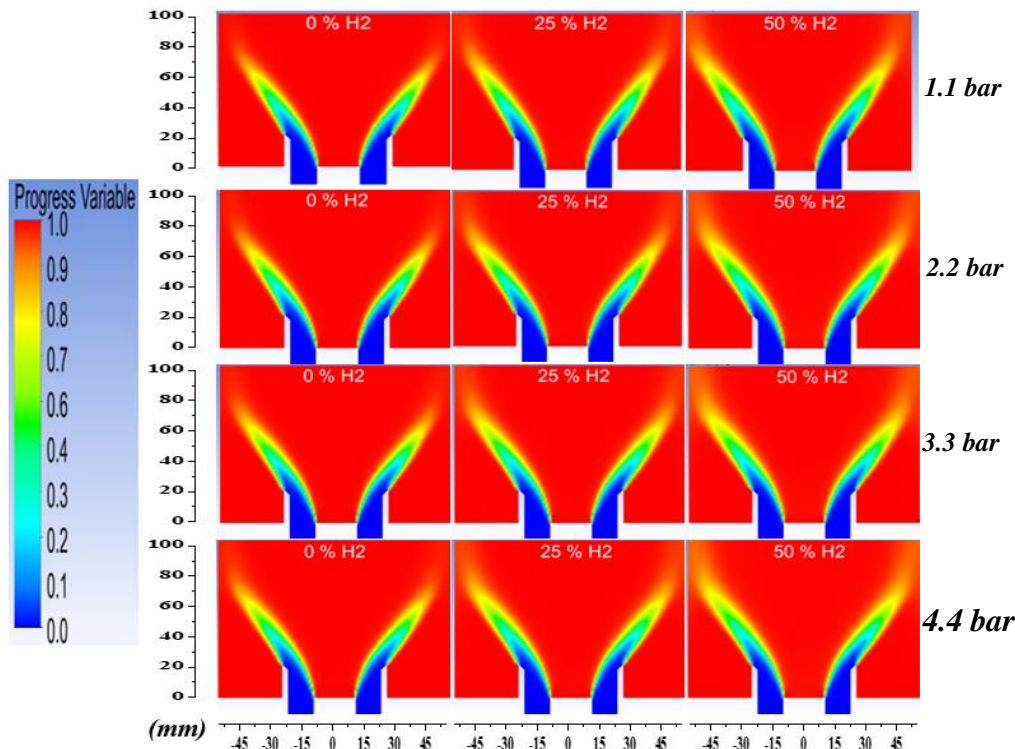


**Fig. 12 Impact of H<sub>2</sub> concentration on the field of the progress variable (1.1, 2.2, 3.3 and 4.4 bar)**

(AFT) as a function of H<sub>2</sub> concentration. At the burner inlet (0 mm < z < 22 mm), the temperature rise is observed indicating the locality of the reaction zone. For the rest of the domain (22mm < z < 400 mm), the temperature profiles are straight lines. This indicates a stabilization of combustion throughout the combustor with a uniform heat distribution. The variation in H<sub>2</sub> content (0%-50%) impacted the maximum temperature (from 1785 K to 1823 K). Although this increase is minimal (around 2%), its repercussions on the appearance of NO<sub>x</sub> must be rigorously analyzed.

For each H<sub>2</sub> value, the effect of inlet pressure (power) on temperature profiles is negligible; the distinction between temperature curves at different pressures for the same H<sub>2</sub> concentration is very difficult. This indicates the great flexibility of HPGSB operation at variable loads (typical behavior of G.T).

For the intermediate concentrations that do not appear in Figure 10 (10 < Vol% H<sub>2</sub> < 20 and 30 < Vol% H<sub>2</sub> < 45), the same developments were found. Increasing H<sub>2</sub> in the reactive mixture increases the maximum temperature reached.

The same conclusions can be drawn from Fig. 11. The temperatures obtained on the radial sections follow the same previous remarks; a slight increase in temperature results from the increase in H<sub>2</sub> concentration as well as a practically invisible elevation of the latter (temperature) as a function of power. Figure 11 showed in particular, the symmetrical aspect of the curves. This indicates a uniform and regular distribution of the heat release zone.

The fields of the Progress Variable "c" are presented in Fig. 12. These images indicate a localization of the reaction zones very close to the burner nozzle outlet (0 mm

< z < 80 mm) for practically all the tested cases. It is noticed that the increase in H<sub>2</sub> concentration resulted in thicker (larger flame front), wider and longer flames. The same observations can be made for the increase in power, the higher the power (translated by the inlet pressure), the thicker, wider and longer the reaction zone. These observations allow us to say that the addition of H<sub>2</sub> allowed the generation of more stable flames with more intense reaction zones. This is the result of the high H<sub>2</sub> flame speeds.

In the end, the impact of substituting CH<sub>4</sub> with H<sub>2</sub> allowed a slight increase in temperature as well as an intensification of the reaction resulting from the higher H<sub>2</sub> flame speeds thus allowing to conclude that HPGSBs can operate on CH<sub>4</sub>-H<sub>2</sub> (up to 50% H<sub>2</sub>) without any restrictions related to the thermal field.

### 3.3 H<sub>2</sub> impact on Velocity

The distribution of the velocity profiles illustrated in Fig. 13 indicates that the increase in H<sub>2</sub> concentration in the reactive mixture has no significant effects. On the three sections analyzed (z= 37 mm, z= 57 mm and z= 77 mm), no noticeable difference is observed between the curves. The same observation was made for the inlet pressures (translated by the power). There is no influence of power on the velocity distribution. This allows us to affirm once again the great operating flexibility of HPGSBs in gas turbines.

The curves obtained are symmetrical with respect to the longitudinal axis of the combustor. This confirms again the development of a symmetrical and stable flow for all the tested cases.

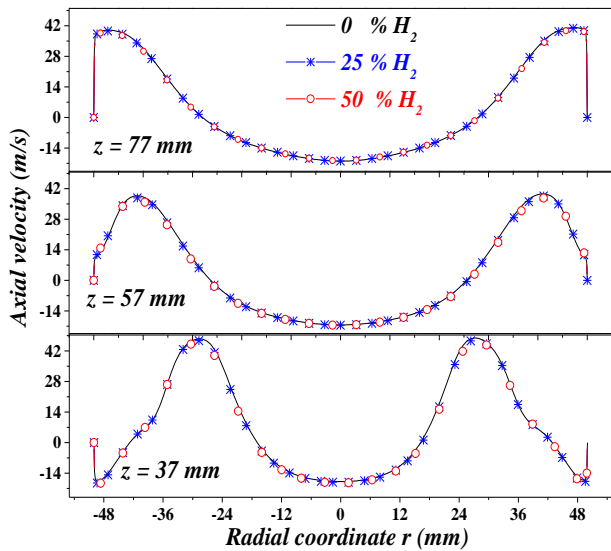


**Fig. 13 Impact of H<sub>2</sub> concentration on velocity distributions along radial cross-sections in the combustor**

Figure 14 shows the presence of CRZs and ORZs near the reaction zone. These allow flame attaching and stabilization. However, it is noticed that the increase in

pressure made the secondary ORZ disappear (case P=4.4 bar corresponding to 168 kW). This is due to the increase in reactant flow rate in the axial direction of the flow thus allowing an intensification of the primary ORZ. On the other hand, the increase in H<sub>2</sub> content did not show any influence on the dynamic field of the flow.

These dynamic fields allow us to conclude that HPGSBs can receive CH<sub>4</sub>-H<sub>2</sub> reactive mixtures up to 50% H<sub>2</sub> without any disturbance in the flow.

### 3.4 H<sub>2</sub> Impact on NO<sub>x</sub>

Increasing the H<sub>2</sub> concentration clearly promoted NO<sub>x</sub> formation (Figure 15). As the H<sub>2</sub> ratio increased, so did the NO<sub>x</sub> levels (exponential evolution). This is due to the lower combustion temperatures of CH<sub>4</sub> (AFT) compared to H<sub>2</sub>, which favors the development of thermal NO<sub>x</sub>.

The largest increase in NO<sub>x</sub> as a function of H<sub>2</sub> concentration was observed at P = 4.4 bar (168 kW). An evolution from 3.2 ppm up to 6.2 ppm was noted, while for the other inlet pressures (1.1 bar, 2.2 bar and 3.3 bar) the increase was less than 2 ppm.

Additionally, increasing the pressure (and thus the power) had the same effect as H<sub>2</sub> but with lower intensity. For the 0% H<sub>2</sub> case, increasing the pressure raised the NO<sub>x</sub>

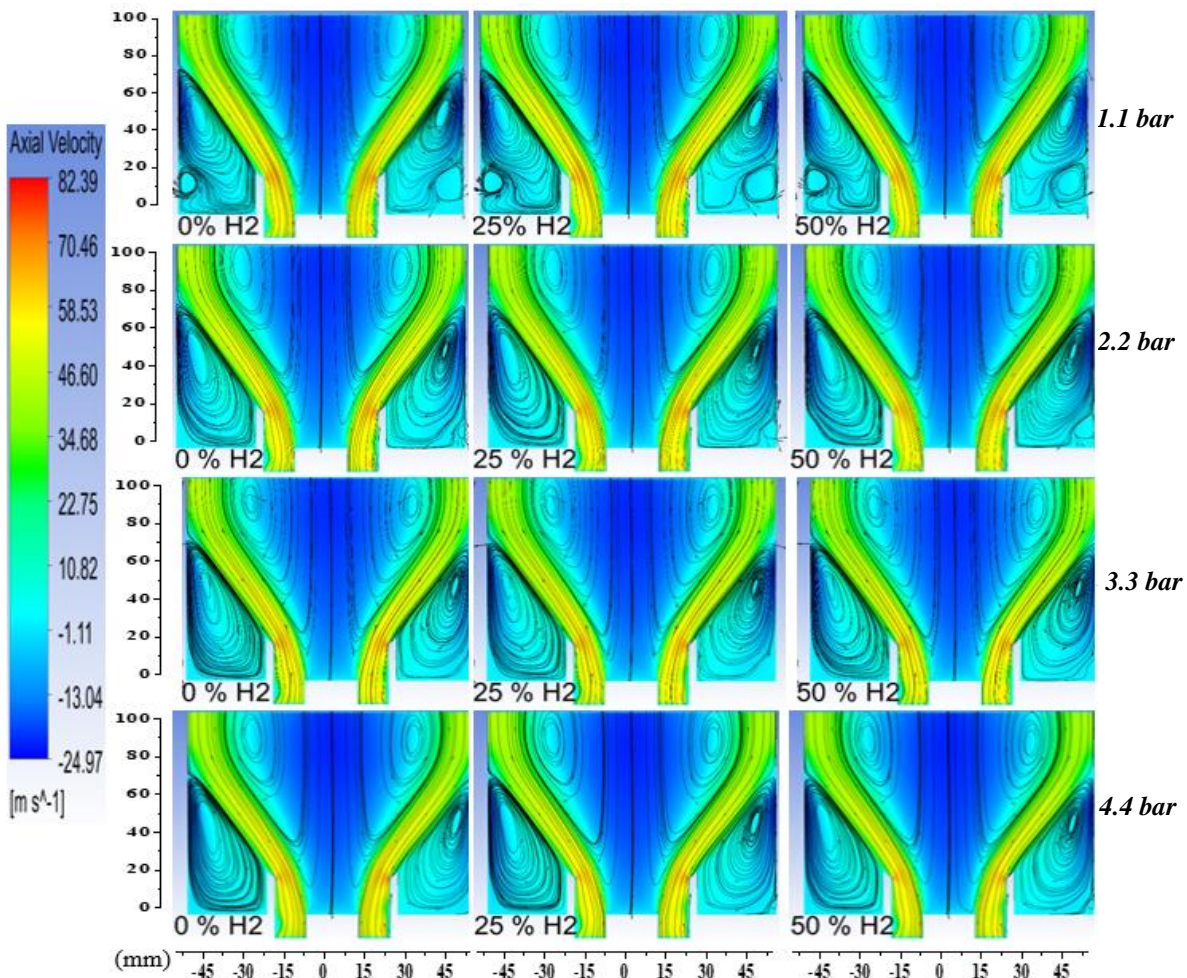


**Fig. 14 Impact of H<sub>2</sub> concentration on stream function and axial velocity (four pressures)**

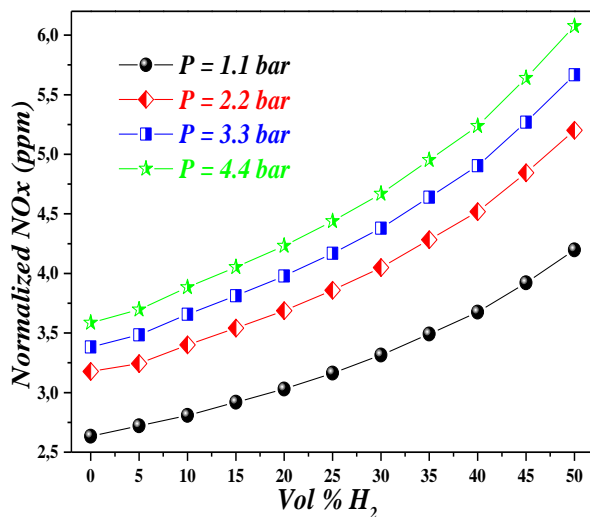


**Fig. 15 Impact of H<sub>2</sub> concentration on normalized NO<sub>x</sub> emission**

by 1 ppm, whereas for 50% H<sub>2</sub>, the NO<sub>x</sub> increased by 2 ppm. This results from the higher flow rate increasing the quantity of reactants, which accelerates combustion and thus favors heat release. Higher operating pressures shorten the residence time of the reactive blend in the combustor chamber. This leads to degraded combustion quality, promoting NO<sub>x</sub> development

Although a NO<sub>x</sub> peak of approximately 6.2 ppm was observed (4.4 bar at 50% H<sub>2</sub>), it remains very acceptable with respect to current regulations. Moreover, several engineering techniques currently exist to reduce pollutant formation such as post-combustion treatment, flue gas recirculation, and others.

In summary, these results allow us to confirm the functionality of HPGBs in H<sub>2</sub>-CH<sub>4</sub> mixtures up to 50%. The thermal, dynamic fields, and NO<sub>x</sub> analysis demonstrate the operational flexibility of this type of combustor used in gas turbines.

#### 4. CONCLUSION

This numerical research investigated the H<sub>2</sub>-CH<sub>4</sub> combustion in HPGB combustors operated in gas turbines (G.T.).

The study includes a literature review focused on previous research works that have investigated HPGBs, a mesh analysis, the validation of the mathematical models used, as well as a detailed examination of the impacts of H<sub>2</sub> concentration on temperature, velocity field, and NO<sub>x</sub> emissions.

The validation of the mathematical models ensured that the Realizable (RANS k-ε) model coupled with the PDF combustion model offered an accurate approach for analyzing the combustion in HPGBs.

The obtained results affirm that the addition of H<sub>2</sub> led to an increase in temperature. 50% H<sub>2</sub> implies a 40 K increase. This value is very acceptable (2%) and does not cause any barrier to the investigated enrichment technique. On the other hand, the H<sub>2</sub>-enriched flame fronts became

wider and thicker with very acceptable dynamic fields, thus offering better combustion stability.

The analyzed power range (42 kW to 168 kW) by varying the inlet pressure (from 1.1 bar to 4.4 bar) did not reveal any major disturbance of the obtained flames. Temperature levels and dynamic fields showed no major variation. This allows us to conclude that HPGBs are designed to operate at wide power ranges, proving good operational flexibility in gas turbines.

As predicted by physical knowledge, the temperature increase had to imperatively promote the formation of NO<sub>x</sub>. The peak observed in our results was 6.2 ppm. This value remains below all current anti-pollution standards.

In conclusion, our results encourage the use of H<sub>2</sub> (up to 50%) in HPGBs without any technical restrictions.

Our perspectives are the use of more accurate mathematical models (Large Eddy Simulation, Detailed Chemistry) and the analysis of different fuels (CH<sub>4</sub>, H<sub>2</sub>, NH<sub>3</sub>, H<sub>2</sub>O vapor, etc.).

#### CONFLICT OF INTEREST

I declare that I have no financial or non-financial conflicts of interest to disclose.

#### REFERENCES

- Adamou, A., Turner, J., Costall, A., Jones, A., & Copeland, C. (2021). Design, simulation, and validation of additively manufactured high-temperature combustion chambers for micro gas turbines. *Energy Conversion and Management*, 248, 114805. <https://doi.org/10.1016/j.enconman.2021.114805>
- Agwu, O., Runyon, J., Goktepe, B., Chong, C. T., Ng, J. H., Giles, A., & Valera-Medina, A. (2020). Visualisation and performance evaluation of biodiesel/methane co-combustion in a swirl-stabilised gas turbine combustor. *Fuel*, 277, 118172. <https://doi.org/10.1016/j.fuel.2020.118172>
- Amani, E., Akbari, M. R., & Shahpouri, S. (2018). Multi-objective CFD optimizations of water spray injection in gas-turbine combustors. *Fuel*, 227, 267-278. <https://doi.org/10.1016/j.fuel.2018.04.093>
- ANSYS Fluent Theory Guide, Release 17.2, ANSYS, Inc. (2016)
- Baej, H., Akair, A., Diyaf, A., Adeilla, S., & Kraiem, A. (2018). Modeling effects of outlet nozzle geometry on swirling flows in gas turbine. <http://dspace.elmergib.edu.ly/xmlui/handle/123456789/67>
- Benaissa, S., Aduane, B., Ali, S. M., Rashwan, S. S., & Aouachria, Z. (2022). Investigation on combustion characteristics and emissions of biogas/hydrogen blends in gas turbine combustors. *Thermal Science and Engineering Progress*, 27, 101178. <https://doi.org/10.1016/j.tsep.2021.101178>

- Boxx, I., Slabaugh, C., Kutne, P., Lucht, R. P., & Meier, W. (2015). 3 kHz PIV/OH-PLIF measurements in a gas turbine combustor at elevated pressure. *Proceedings of the Combustion Institute*, 35(3), 3793-3802. <https://doi.org/10.1016/j.proci.2014.06.090>
- Bulat, G., Fedina, E., Fureby, C., Meier, W., & Stopper, U. (2015). Reacting flow in an industrial gas turbine combustor: LES and experimental analysis. *Proceedings of the Combustion Institute*, 35(3), 3175-3183. <https://doi.org/10.1016/j.proci.2014.05.015>
- Chen, F., Ruan, C., Yu, T., Cai, W., Mao, Y., & Lu, X. (2019). Effects of fuel variation and inlet air temperature on combustion stability in a gas turbine model combustor. *Aerospace Science and Technology*, 92, 126-138. <https://doi.org/10.1016/j.ast.2019.05.052>
- Chen, Y., & Driscoll, J. F. (2016). A multi-chamber model of combustion instabilities and its assessment using kilohertz laser diagnostics in a gas turbine model combustor. *Combustion and Flame*, 174, 120-137. <https://doi.org/10.1016/j.combustflame.2016.08.022>
- Emami, M. D., Shahbazian, H., & Sunden, B. (2019). Effect of operational parameters on combustion and emissions in an industrial gas turbine combustor. *Journal of Energy Resources Technology*, 141(1), 012202. <https://doi.org/10.1115/1.4040532>
- Erdener, B. C., Sergi, B., Guerra, O. J., Chueca, A. L., Pambour, K., Brancucci, C., & Hodge, B. M. (2023). A review of technical and regulatory limits for hydrogen blending in natural gas pipelines. *International Journal of Hydrogen Energy*, 48(14), 5595-5617. <https://doi.org/10.1016/j.ijhydene.2022.10.254>
- İlbaş, M., Karyeyen, S., & Yilmaz, İ. (2016). Effect of swirl number on combustion characteristics of hydrogen-containing fuels in a combustor. *International Journal of Hydrogen Energy*, 41(17), 7185-7191. <https://doi.org/10.1016/j.ijhydene.2015.12.107>
- Kruse, S., Kerschgens, B., Berger, L., Varea, E., & Pitsch, H. (2015). Experimental and numerical study of MILD combustion for gas turbine applications. *Applied Energy*, 148, 456-465. <https://doi.org/10.1016/j.apenergy.2015.03.054>
- Kurata, O., Iki, N., Inoue, T., Matsunuma, T., Tsujimura, T., Furutani, H., Kawano, M., Arai, K., Okafor, E. C., Hayakawa, A. & Kobayashi, H. (2019). Development of a wide range-operable, rich-lean low-NO<sub>x</sub> combustor for NH<sub>3</sub> fuel gas-turbine power generation. *Proceedings of the combustion Institute*, 37(4), 4587-4595. <https://doi.org/10.1016/j.proci.2018.09.012>
- Lee, M. C., Yoon, J., Joo, S., Kim, J., Hwang, J., & Yoon, Y. (2015). Investigation into the cause of high multi-mode combustion instability of H<sub>2</sub>/CO/CH<sub>4</sub> syngas in a partially premixed gas turbine model combustor. *Proceedings of the Combustion Institute*, 35(3), 3263-3271. <https://doi.org/10.1016/j.proci.2014.07.013>
- Li, S., Zhang, S., Zhou, H., & Ren, Z. (2019). Analysis of air-staged combustion of NH<sub>3</sub>/CH<sub>4</sub> mixture with low NO<sub>x</sub> emission at gas turbine conditions in model combustors. *Fuel*, 237, 50-59. <https://doi.org/10.1016/j.fuel.2018.09.131>
- Liu, H., Wang, Y., Yu, T., Liu, H., Cai, W., & Weng, S. (2020). Effect of carbon dioxide content in biogas on turbulent combustion in the combustor of micro gas turbine. *Renewable Energy*, 147, 1299-1311. <https://doi.org/10.1016/j.renene.2019.09.014>
- Liu, Y., Sun, X., Sethi, V., Nalianda, D., Li, Y. G., & Wang, L. (2017). Review of modern low emissions combustion technologies for aero gas turbine engines. *Progress in Aerospace Sciences*, 94, 12-45. <https://doi.org/10.1016/j.paerosci.2017.08.001>
- Lokini, P., Roshan, D. K., & Kushari, A. (2019). Influence of swirl and primary zone airflow rate on the emissions and performance of a liquid-fueled gas turbine combustor. *Journal of Energy Resources Technology*, 141(6), 062009. <https://doi.org/10.1115/1.4042410>
- Mahto, N., & Chakravarthy, S. R. (2022). Response surface methodology for design of gas turbine combustor. *Applied Thermal Engineering*, 211, 118449. <https://doi.org/10.1016/j.applthermaleng.2022.118449>
- Masrouri, M., Tahsini, A. M., & Vahabi, S. E. (2023). Coating roughness impact on the combustion chambers life of the turbo engines. *Proceedings of the Institution of Mechanical Engineers, Part G: Journal of Aerospace Engineering*, 09544100231181209. <https://doi.org/10.1177/09544100231181209>
- Moraes, R. C., Dias, M. A., & Mendes Neto, L. J. (2022). Gas turbine combustor CFD study and single-objective DoE optimization. *Numerical Heat Transfer, Part A: Applications*, 82(11), 700-715. <https://doi.org/10.1080/10407782.2022.2083863>
- Murthy, M. S. N., Bhadkamkar, N., Penumarti, A., Prabhu, S. V., & Sreedhara, S. (2018). Numerical investigation of swirl flow using different swirlers in a real-life gas turbine combustor. *Journal of Flow Visualization and Image Processing*, 25(2). <https://doi.org/10.1615/JFlowVisImageProc.2018027771>
- Nemitallah, M. A., Rashwan, S. S., Mansir, I. B., Abdelhafez, A. A., & Habib, M. A. (2018). Review of novel combustion techniques for clean power production in gas turbines. *Energy & Fuels*, 32(2), 979-1004. <https://doi.org/10.1021/acs.energyfuels.7b03607>
- Okafor, E. C., Somarathne, K. K. A., Hayakawa, A., Kudo, T., Kurata, O., Iki, N., & Kobayashi, H. (2019). Towards the development of an efficient

- low-NO<sub>x</sub> ammonia combustor for a micro gas turbine. *Proceedings of the combustion institute*, 37(4), 4597-4606. <https://doi.org/10.1016/j.proci.2018.07.083>
- Ouali, S., Bentebbiche, A. H., & Belmrabet, T. (2016). Numerical simulation of swirl and methane equivalence ratio effects on premixed turbulent flames and NO<sub>x</sub> apparitions. *Journal of Applied Fluid Mechanics*, 9(2), 987-998. <https://doi.org/10.18869/acadpub.jafm.68.225.22603>
- Pashchenko, D. (2024). Ammonia fired gas turbines: Recent advances and future perspectives. *Energy*, 290, 130275. <https://doi.org/10.1016/j.energy.2024.130275>
- Psomoglou, I. (2023). *Influence of surface roughness on burner characteristics and combustion performance of AM combustors* [Doctoral dissertation, Cardiff University]. <https://orca.cardiff.ac.uk/id/eprint/162894>
- Rajabi, V., & Amani, E. (2019). A computational study of swirl number effects on entropy generation in gas turbine combustors. *Heat Transfer Engineering*, 40(3-4), 346-361. <https://doi.org/10.1080/01457632.2018.1429056>
- Reale, F., & Sannino, R. (2021). Water and steam injection in micro gas turbine supplied by hydrogen enriched fuels: Numerical investigation and performance analysis. *International Journal of Hydrogen Energy*, 46(47), 24366-24381. <https://doi.org/10.1016/j.ijhydene.2021.04.169>
- Runyon, J. O. N. (2017). *Gas turbine fuel flexibility: pressurized swirl flame stability, thermoacoustics, and emissions* [Doctoral dissertation, Cardiff University]. <https://orca.cardiff.ac.uk/id/eprint/100686>
- Runyon, J., Giles, A., Marsh, R., Pugh, D., Goktepe, B., Bowen, P., & Morris, S. (2020). Characterization of additive layer manufacturing swirl burner surface roughness and its effects on flame stability using high-speed diagnostics. *Journal of Engineering for Gas Turbines and Power*, 142(4), 041017. <https://doi.org/10.1115/1.4044950>
- See, Y. C., & Ihme, M. (2015). Large eddy simulation of a partially-premixed gas turbine model combustor. *Proceedings of the Combustion Institute*, 35(2), 1225-1234. <https://doi.org/10.1016/j.proci.2014.08.006>
- Syred, N., Morris, S. M., Bowen, P. J., Valera-Medina, A., & Marsh, R. (2015). *Preliminary results from a high pressure optical gas turbine combustor model with 3D viewing capability*. 53rd AIAA Aerospace Sciences Meeting. <https://doi.org/10.2514/6.2015-1655>
- Valera-Medina, A., Marsh, R., Runyon, J., Pugh, D., Beasley, P., Hughes, T., & Bowen, P. (2017). Ammonia-methane combustion in tangential swirl burners for gas turbine power generation. *Applied Energy*, 185, 1362-1371. <https://doi.org/10.1016/j.apenergy.2016.02.073>
- Zhang, H., Zhang, Z., Xiong, Y., Liu, Y., & Xiao, Y. (2018, June). *Experimental and numerical investigations of MILD combustion in a model combustor applied for gas turbine*. Turbo Expo: Power for Land, Sea, and Air. American Society of Mechanical Engineers. <https://doi.org/10.1115/GT2018-76253>
- British Standard, I. S. O. (1996). 11042-1: 1996, Gas turbines. Exhaust gas emission Measurement and evaluation. British Standards Institution, UK.